Landscape Dynamics Assessment of Mount Namuli Region

Montfort Frédérique

Grinand Clovis

December 2020

nitidæ filières & territoires

www.nitidae.org

Table of contents

Executive summary

This report presents the Landscape Dynamics Assessment (LDA) of Mount Namuli region based on satellite-observed land cover and vegetation change. This assessment is composed of four analysis: a Land Use and Land Cover mapping, an analysis of land degradation, an analysis of historical deforestation, and an analysis of risks of deforestation.

The land use and land cover mapping of the Mount Namuli region for the year 2020, using Sentinel-2 imagery has been used to update the statistics on land cover categories in the region. This analysis notably, allows to update the extent of remaining forest patches of moist evergreen forest, estimated in 2020 at 785 ha. We found that 17% of the 2018 forest cover has been lost between 2018 and 2020 years.

We characterized and mapped drivers of land productivity changes over the 2000-2016 period of the Mount Namuli region using remote sensing data. Land productivity change analysis allows us to study all changes in vegetation natural or cultivated and their potential factors. This analysis evidenced that 23% of the study area display a land productivity decreased and a large part of this negative trend could mainly be related to anthropogenic activities (agriculture expansion and tea plantation productivity decrease).

We mapped forest extent and deforestation in the Namuli core area over the 2000-2020 period, using Landsat images. More than 40% (i.e. 568 ha) of the forested areas in the Namuli core area was lost between 2000 and 2020. The Namuli core area had suffered important deforestation since mainly 2009, losing on average 48 ha per year, between 2009 and 2020 – this is an average annual deforestation rate of 4.7%. Based on this analysis of historical deforestation and comprehension of the deforestation drivers, we mapped future threatened forest patches in the Namuli core area. All forest patches located in low slope areas (< 13%) present a high risk of deforestation, conversely high sloped areas are less threatened.

1_Introduction

Mount Namuli, Mozambique's second highest peak, at 2,419 meters, is part of the belt of granite rock outcrops, inselbergs and mountains, running NE-SW across Nampula and Zambezia provinces and including Mt Inago (1804 m) and Ribaue Mountains (Mt Ribaue and Mt M'Palawe – 1675 m). Mount Namuli's slopes covered by a mosaic of forests, grassland and cropland, are incredibly diverse but threatened by the expansion of Irish potato cultivation.

Since October 2018 Nitidæ has joined Lupa and Legado to reinforce the partnership for the preservation of Mount Namuli and community development in Namuli's surrounding communities in the project Legado: Namuli. The main objective of this project is to establish an official classification in the community protected area of Mount Namuli. By working with communities living around the mountain and developing with them a long-term natural resource management strategy, the project aims to put an end to deforestation in high altitude forests, to guarantee the resilience of the biodiversity of Mount Namuli and increase local economy. Since 2019, Nitidæ has also been involved in the Legado: Ribaue project for the biodiversity preservation and community development in Ribaue Mountains.

This report presents the Landscape Dynamics Assessment (LDA) of Mount Namuli region based on satellite-observed land cover and vegetation change. This assessment is composed of four analysis:

- *Land use and land cover mapping* of Mount Namuli region for the year 2020: this section aims to update the 2018 LULC map using Sentinel 2 image.
- *Analysis of land degradation*: this section aims to assess the underlying factors (human or climatic) in vegetation (natural or cultivated) productivity changes over the 2000-2016 period, in order to assess land degradation of Mount Namuli region.
- *Analysis of historical deforestation*: this section aims to map forest extent and deforestation in the Namuli core area over the 2000-2020 period on the basis of Landsat images.
- *Analysis of risks of future deforestation*: this section aims to map future threatened forest patches in the Namuli core area, based on historical deforestation and comprehension of the deforestation drivers.

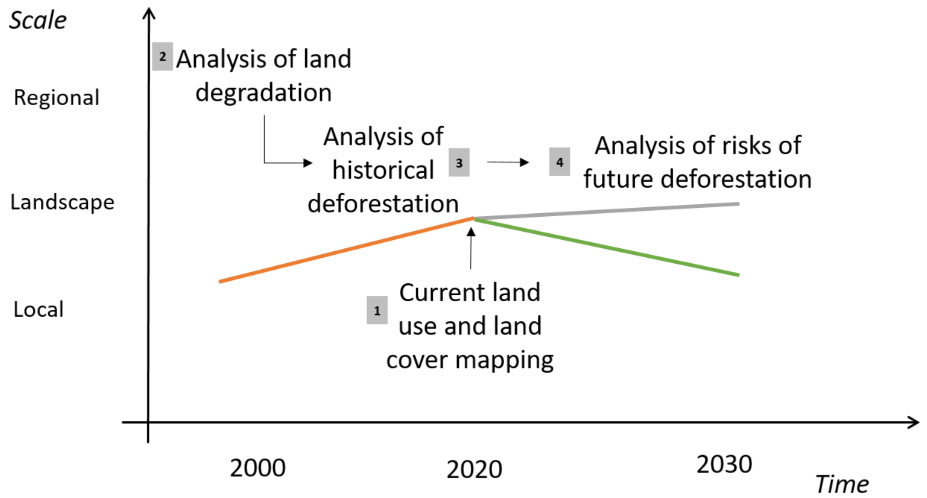

Figure 1 : Landscape Dynamics Assessment

2_ Context

The Mount Namuli Massif is located in the north of Gurué, in the northwest of the Zambezia province and 150 km from the Malawi border (Figure 2). The tea production is the main economic activity. This was initiated by the Portuguese in 1930, then in 1980-90 managed by the state and currently managed by private Mozambican and other companies (Timberlake et al., 2009). Apart from a few contract jobs in tea plantations, people live mainly from subsistence and local market agriculture.

The Mount Namuli Massif, covers an area of about 200 km² at an altitude above 1200 m (Timberlake et al., 2009). The highest point of the massif, Mount Namuli, reaches 2,419 m. It is the second highest peak in Mozambique after Mount Binga (2,436 m) located in the Chimanimani National Reserve (Manica Province). The region surrounding Mount Namuli is inhabited by local communities who rely on it heavily for ecosystem services. Although, the area's biodiversity is greatly threatened by conversion of forests and grasslands by these communities for subsistence and local market agriculture. There is minimal local government involvement in the area for conservation activities or social services, and thus there has been no effective management of natural resources. Mount Namuli is relatively small in extent but incredibly diverse and a part of the unique mountain island chain of inselbergs in northern Mozambique. Rates of habitat loss, particularly across high conservation value areas above 1,200 meters, are increasing, driven primarily by the introduction of crops, such as the Irish potato, which exhaust the soils. The high rates of forest conversion underway on the mountain's upper slopes must be halted immediately and long-term plans for natural resource management must be implemented if Mount Namuli's remaining biodiversity is to be retained.

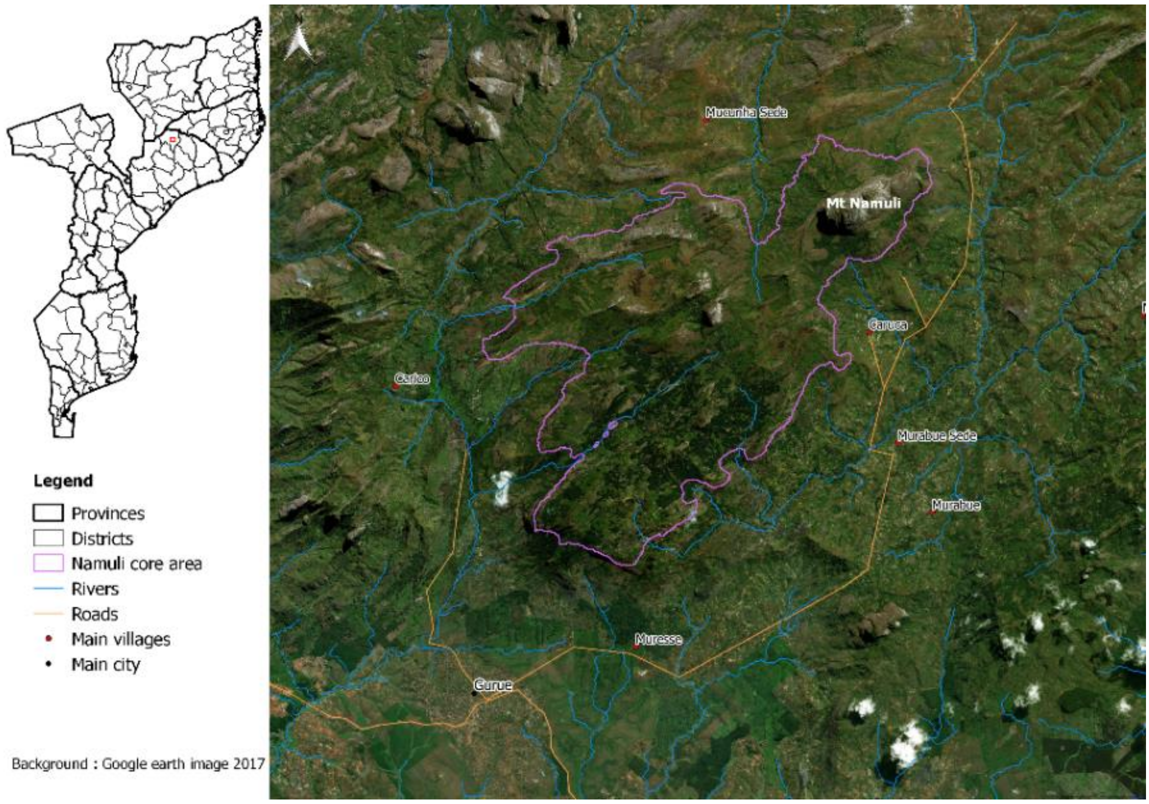

Figure 2 : Location of Namuli area

3_ LULC map update

The objective of this section is to map the land use and land cover of Mount Namuli and surrounding for the year 2020 to update the 2018 LULC map. The LULC map update allows the monitoring of change in the extent of moist evergreen forest and estimated deforestation rates. This section describes the various steps that have been implemented for the LULC map update, from the acquisition of satellites images to the final results. The statistics presented in this section may differ from those presented in the historical deforestation analysis section due to the different resolutions of the images used (Landsat: 30 m and Sentinel 2: 10 m).

3.1. Methodology

The methodology is based on a remote sensing methodology and is presented in the report of the 2018 LULC map (Montfort & Grinand, 2018):

- Satellite image collection:
  - Production of cloud-free and shadow free Sentinel 2 (10 m resolution, bands: 2, 3, 4, 8, 11, 12) with Google Earth Engine,
  - Image acquired between June and August 2018 (3 month period – Dry season)
- Data pre-processing: three categories of variables have been used
  - Sentinel 2 spectral bands,
  - Soil, water and vegetation indices (NDVI, SAVI, NDWI),
  - Topographic indices such as altitude, slope and the relative height.
- Identification of land use typology,
- Delineation of training plots: 598 plots were collected,
- Supervised classification of land use using a machine learning algorithm (Random Forest)
- Post-processing steps (Sieving).

The methodology is summarized in the following figure:

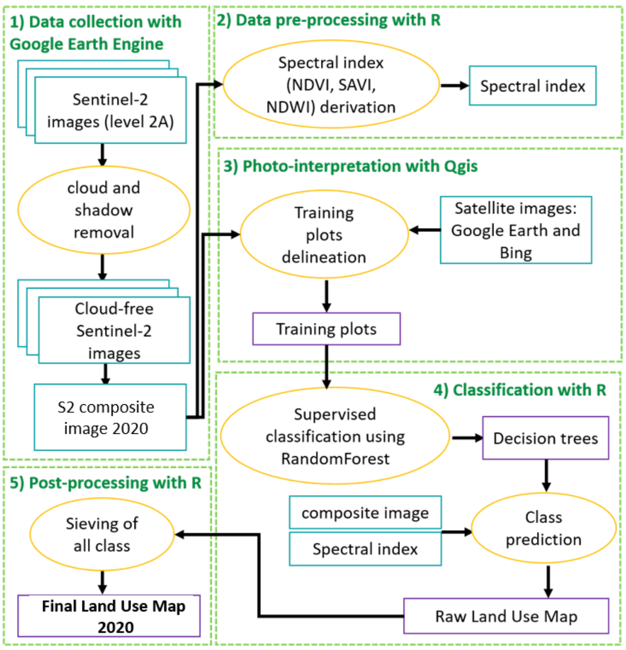

Figure 3 : Processing chain applied for the land use mapping

3.2. Results

3.2.1. Land Use and Land Cover map of Mount Namuli region

The LULC map for 2020 is presented in Figure 4 and LULC statistics in Table 1. The landscape is largely dominated by agricultural land composed by cropland, fallow and some areas of settlement, which accounts for 37 % (28 547 ha) of the total area studied. Secondary vegetation or woodland is the second most represented category with an area of 20 396 ha or 26 % of the total area. Tea and tree plantation cover an area of 9 275 ha or 12 %. Forest land covers only 1.8 % of the study area, mainly located above 1400 m altitude.

Comparison of the 2018 and 2020 land-use maps of Mount Namuli region shows that in two years, we observe a decrease in forest cover (loss of 22% between 2018 and 2020) and an increase in the area of secondary vegetation (gain of 11%), macadamia plantations (gain of 127%), irrigated cultivation (gain of 21%), urban areas and settlement (gain of 23%).

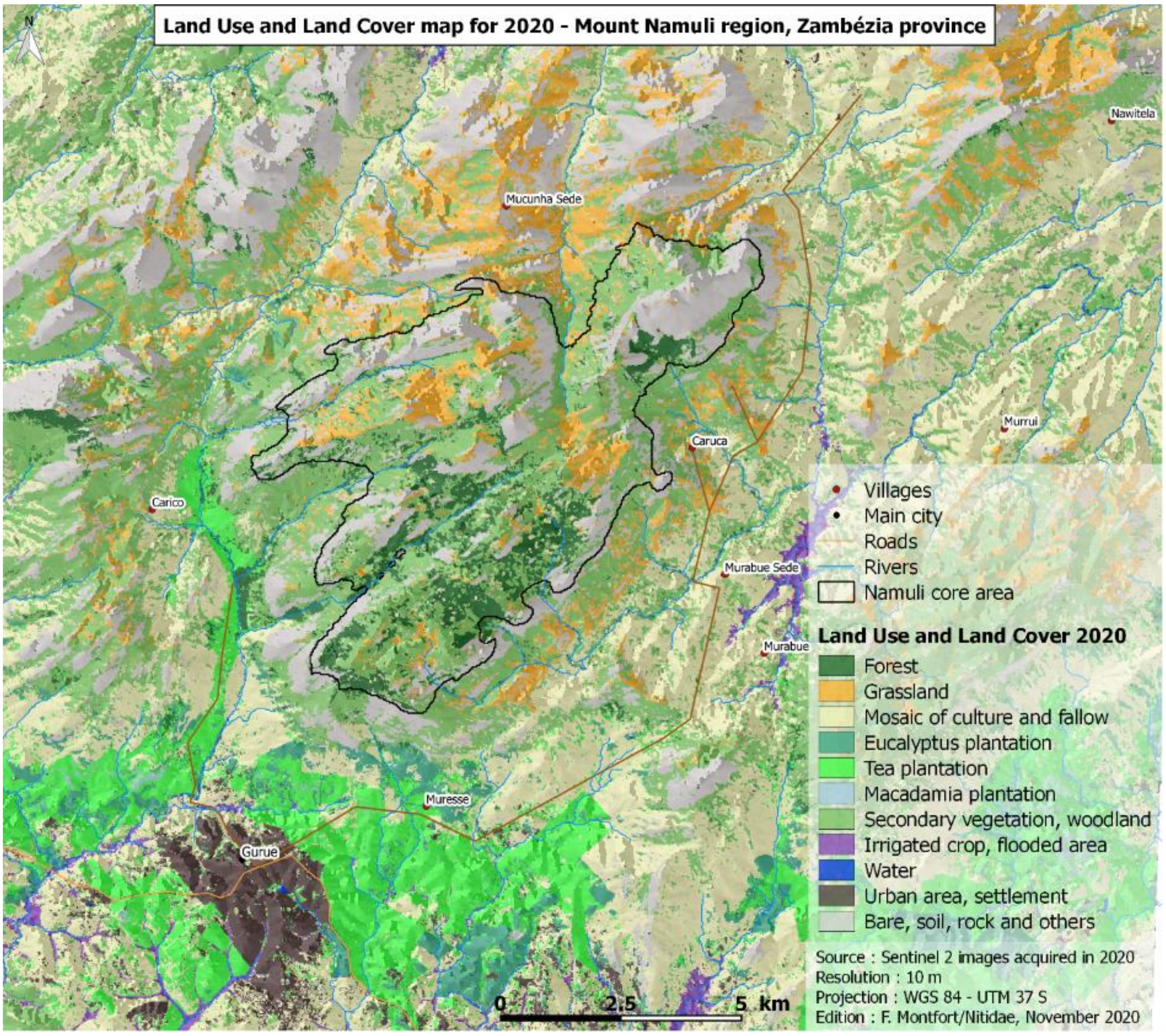

Figure 4 : Land Use and Land Cover map of the Mount Namuli and surroundings (2020)

Table 1: Area and proportion of land use and land cover classes of Mount Namuli and surroundings area calculated from the 2020 LULC map and land-use dynamics - increase (↗), decrease (↘) or no change (=) - between 2018 and 2020

Code	Short Name	Area (ha)	% of total area	LULC dynamics between 2018 and 2020
1	Forest	1 409	1.8	↘
2	Grassland	4 406	5.7	=
3	Mosaic of culture and fallow	28 547	37.0	=
4	Eucalyptus plantation	2 092	2.5	=
5	Tea plantation	6 879	8.9	=
6	Macadamia plantation	304	0.4	↗
7	Secondary vegetation, woodland	20 396	26.4	↗
8	Irrigated crop, Flooded area	1 591	2.1	↗
9	Water	77	0.1	=
10	Urban area, Settlement	1 746	2.3	↗
11	Bare soil, rock, sands	9 735	12.6	=
Total		77 753	100	

3.2.2. Land Use and Land Cover Change map of the Namuli core area

The LULC map for 2020 is presented in Figure 5 and LULC statistics in Table 2. Remaining moist evergreen forest areas cover 785 ha and account for 16 % of the total area. **Areas of secondary vegetation of woodland can be natural areas or areas partially cleared, cultivated or frequently affected by fire, these areas cover 2006 ha or 40 % of the core area. Grassland covers 607 ha (12 % of total area).** Cropland and fallow in the core area that could be detected in the analysis, cover a total area of 71 ha and patches do not exceed 0.5 ha.

Comparison of the 2018 and 2020 land-use maps shows that, 164 ha (17% of the 2018 forest cover) have been lost in two years. These forest patches were probably converted to cropland but a cropland expansion was not detected in the analysis. Results show that forest pixels were mainly converted to secondary vegetation pixels. Indeed, due to their smaller size, some cropland may not have been detected during the analysis or may have been confused with secondary vegetation.

Table 2: Area and proportion of land use and land cover classes in the Namuli core area, calculated from the LULC 2018 and 2020 map

Code	Short Name	2018		2020		LULC dynamics between 2018 and 2020
		Area (ha)	% of total area	Area (ha)	% of total area	
1	Forest (Montane Forest)	949	18.9	785	15.6	↘
2	Grassland	623	12.4	607	12.1	=
3	Mosaic of culture and fallow	126	2.5	71	1.4	↘
7	Secondary vegetation, woodland	1 735	34.6	2006	40.0	↗
11	Bare soil, rocks, sands	1 586	31.6	1553	30.1	=
Total		5 020	100	5 020	100	

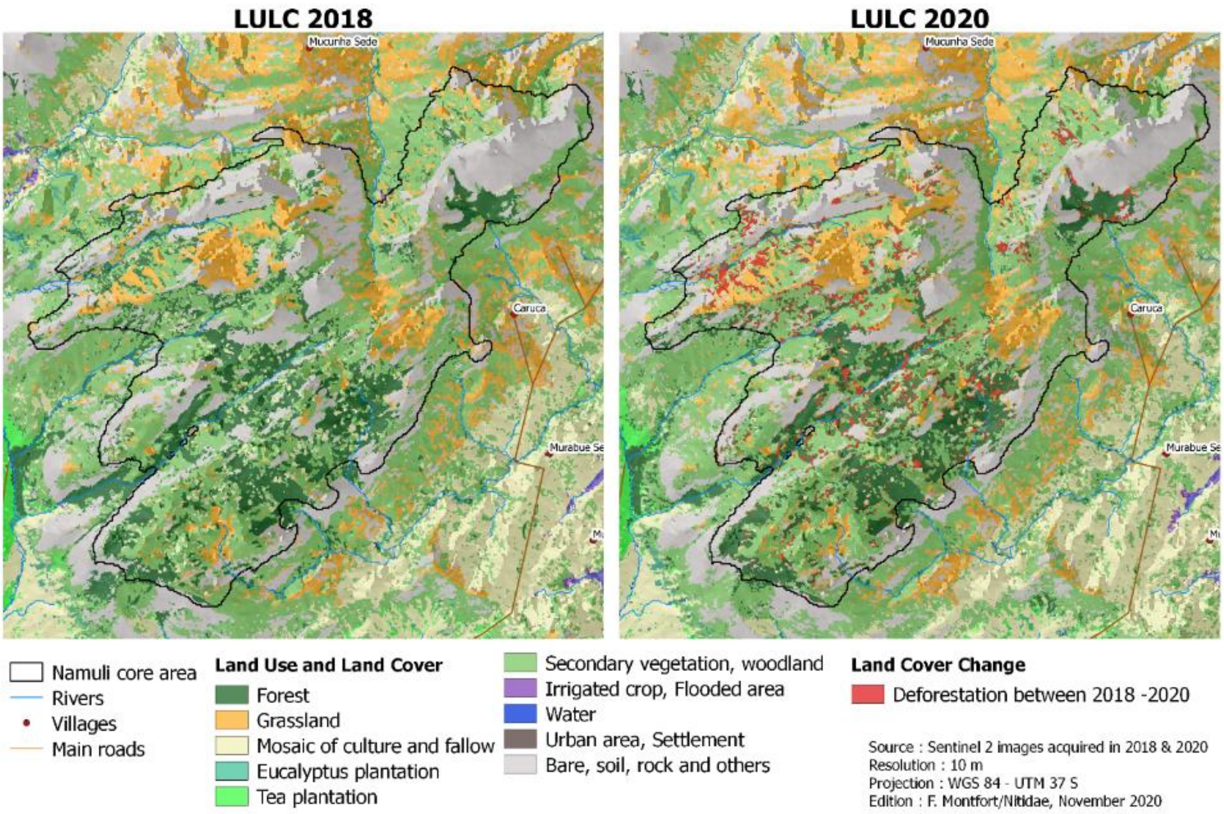

Figure 5 : Land Use and Land Cover map (2018 and 2020) of the Namuli core area and deforestation between 2018 and 2020

4_ Land degradation analysis

Vegetation variations observed over long periods is indeed a good indicator of ecological conditions or changing production conditions - soil fertility, water availability, and land use. It is therefore a measure of the response of ecosystems to the external impacts, whether they are induced by human activity or natural variability, and provides information on land condition. The reduction or loss of productivity, biological and/or economic, is a common denominator of the various definitions of land degradation. Land productivity is therefore an essential piece of information for degradation monitoring.

Remote sensing data have been recognized for several decades as a powerful tool to map vegetation cover. In particular, the Normalized Difference Vegetation Index (NDVI) is an index of plant greenness or potential photosynthetic activity. Because NDVI has shown consistent correlation with vegetation biomass and dynamics in various ecosystems worldwide, NDVI trends integrated over a time period can be used as a proxy to monitor changes in land productivity.

The objective of this section is to analyze land productivity underlying factors (climatic or human) in order to assess land degradation of Mount Namuli and surrounding. This analysis allows (1) to identify areas of significant changes in land productivity during the period, (2) to determine the direction of these changes, namely either an increase in land productivity potentially reflecting a trend towards restoration of the vegetation or a decrease reflecting a degradation of the vegetation, and (3) to assess potential drivers of change.

This analysis is carried out on a coarse spatial resolution (250 m), but provides an overview of the major changes (all vegetation changes and not only changes related to deforestation) that occurred place in the region and an identification of the main drivers of change.

4.1. Methodology:

The methodology is based on Montfort et al.'s (2020) method. Land productivity changes were first analyzed using NDVI time-series (2000–2016 – MODIS data, 250 m) and a statistical trend analysis based on an Ordinary-Least Square (OLS) regression over the period. The OLS were applied to each pixel of the time series. Each pixel was then classified according to the slope (positive or negative) and the p-value with a significance threshold of 95% ($p\text{-value}<0.05$).

Then a two-step framework was used to understand the main factors of these productivity changes: first the climate effect was extracted using rainfall (CHIRPS, 0.05°) and temperature (CRU, 0.5°) datasets, and then the human activities effects were extracted using LULC data and ground knowledge. Each pixel was classified using a classification scheme based on the slope of the NDVI trend and the LULCC categories. Each change factor represents the main potential factor based on ground observations for productivity changes related to each LULCC category. The methodology is summarized in figure 6.

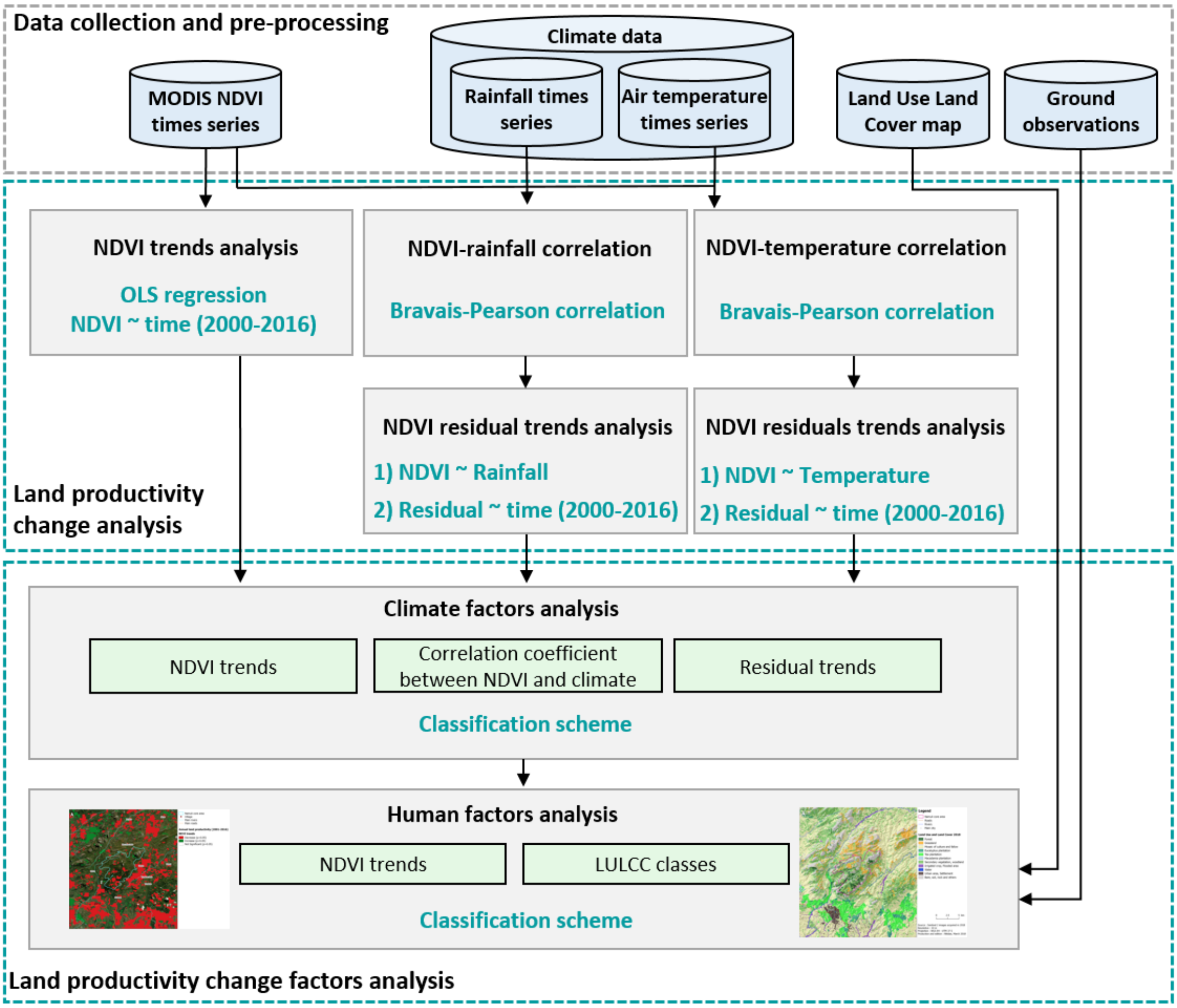

Figure 6 : Flowchart of the land productivity change analysis

4.2. Results

4.2.1. Annual land productivity

Around 73% of the study area (52 955 ha) shows no significant land productivity change over the 2000-2016 period (Figure 7). Some 23.4% (16 976) of the total area display a decrease in land productivity (degradation of vegetation), while only 3.5% (2 524 ha) shows increase in land productivity (vegetation restoration).

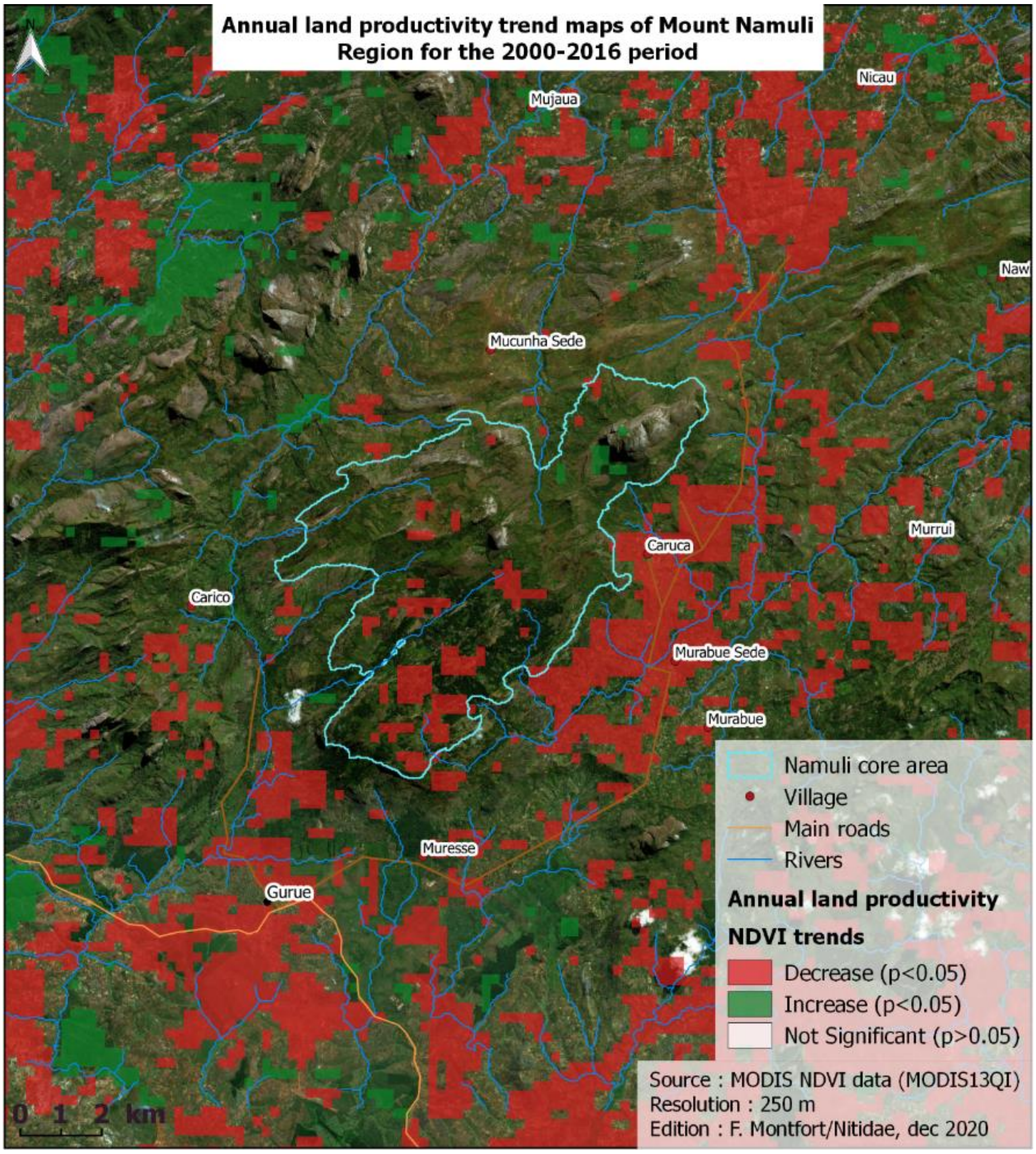

Figure 7 : Annual land productivity trend maps of Mount Namuli and surroundings calculated for the 2000-2016 period

4.2.2. Land productivity decrease factors

Human activities remain the dominant factors in land productivity decrease (Figure 8, Table 3). This decrease can be mainly explained by agriculture expansion or productivity decline in cropland (52.4 % the total decrease trend), productivity decline in tea plantations or clearcutting (12.1 %), past deforestation or woodland productivity decline (11.8 %).

To the east of the Namuli core area, the area of land productivity decrease corresponds to an area of cropland densification and settlement on previously sparsely inhabited areas. Within the core area the decrease in land productivity corresponds to areas of deforestation for the cultivation of Irish potato (Batata reno) since the 2000s, due to the displacement of populations to the top of the massif linked to the loss of soil fertility lower down and the development of an attractive market linked to potatoes.

In the valley, several areas of productivity decline were linked to the abandonment of tea plantations in the early 2000s, which were then cut, burnt and converted into (Figure 9):

- Settlement areas, close to the town of Gurué;

- Fields for growing maize or cassava (family or commercial agriculture);

- In a Macadamia orchard: in the north-west of Gurué, establishment of the company Murrimo Macadamia, which produces macadamia nuts, maize and beans.

Some tea plantations are still being exploited (harvested and pruned), but show a decrease in plant productivity. This is the case of plantations established in the 1940s and currently very degraded, located near the town of Gurué. This decline in land productivity can be linked to several factors, including the age of the plantations, diseases affecting the plants, but also soil degradation or the diminution of shadow tree density in tea plantation.

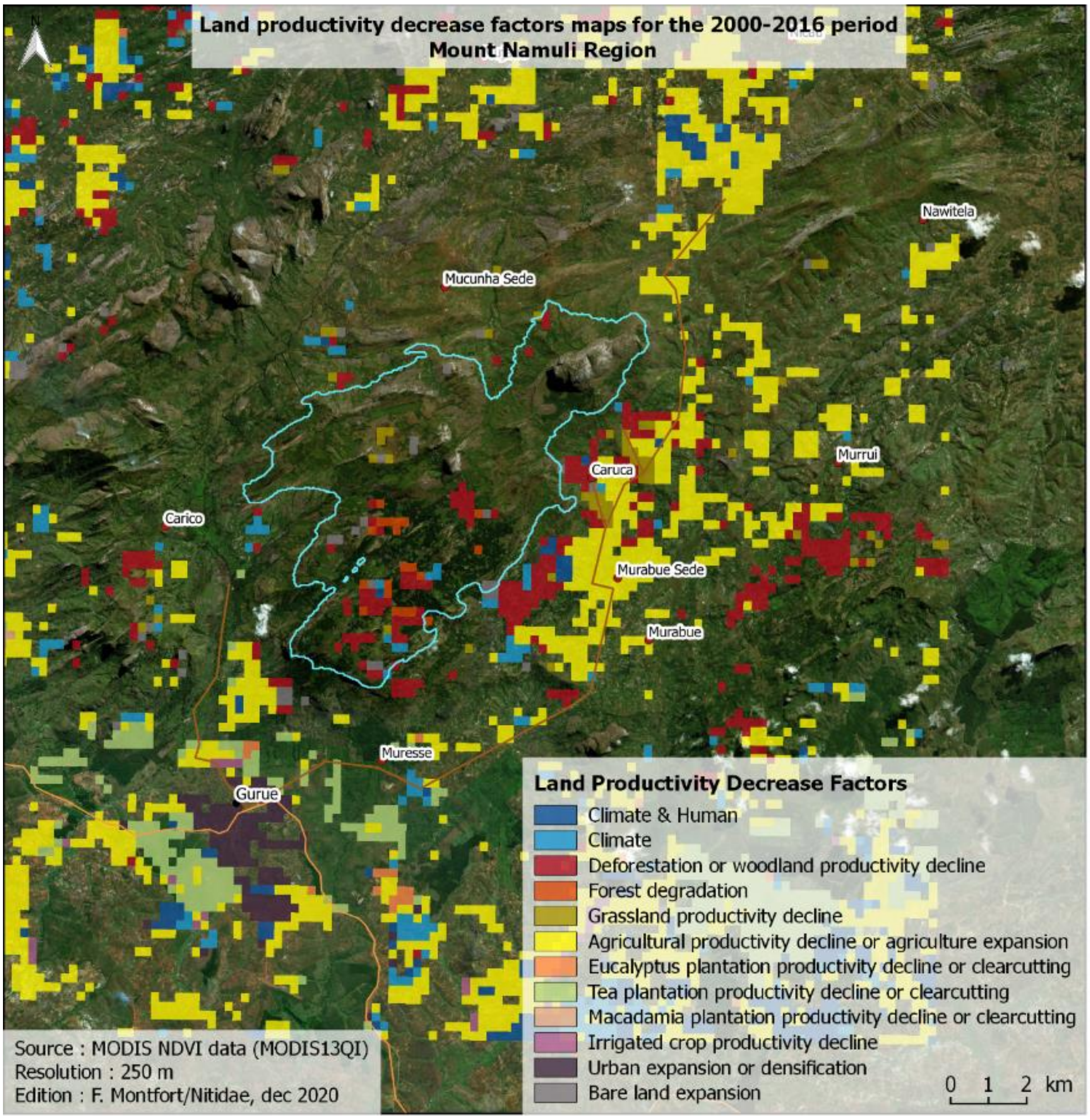

Figure 8 : Spatial distribution of the main drivers of land productivity decreases.

Table 3: Distribution of main factors of land productivity decreases.

Potential land productivity factors	Hectares	% decrease
Agricultural productivity decline or agriculture expansion	8 898	52,4
Tea plantation productivity decline or clearcutting	2 046	12,1
Deforestation or woodland productivity decline	2 009	11,8
Climate + Others	1 373	8,1
Climate	1 146	6,8
Urban expansion or densification	534	3,1
Grassland productivity decline	283	1,7
Bare land expansion	269	1,6
Irrigated crop productivity decline	153	0,9
Eucalyptus plantation productivity decline or clearcutting	111	0,7
Deforestation or forest degradation	97	0,6
Macadamia plantation productivity decline or clearcutting	56	0,3

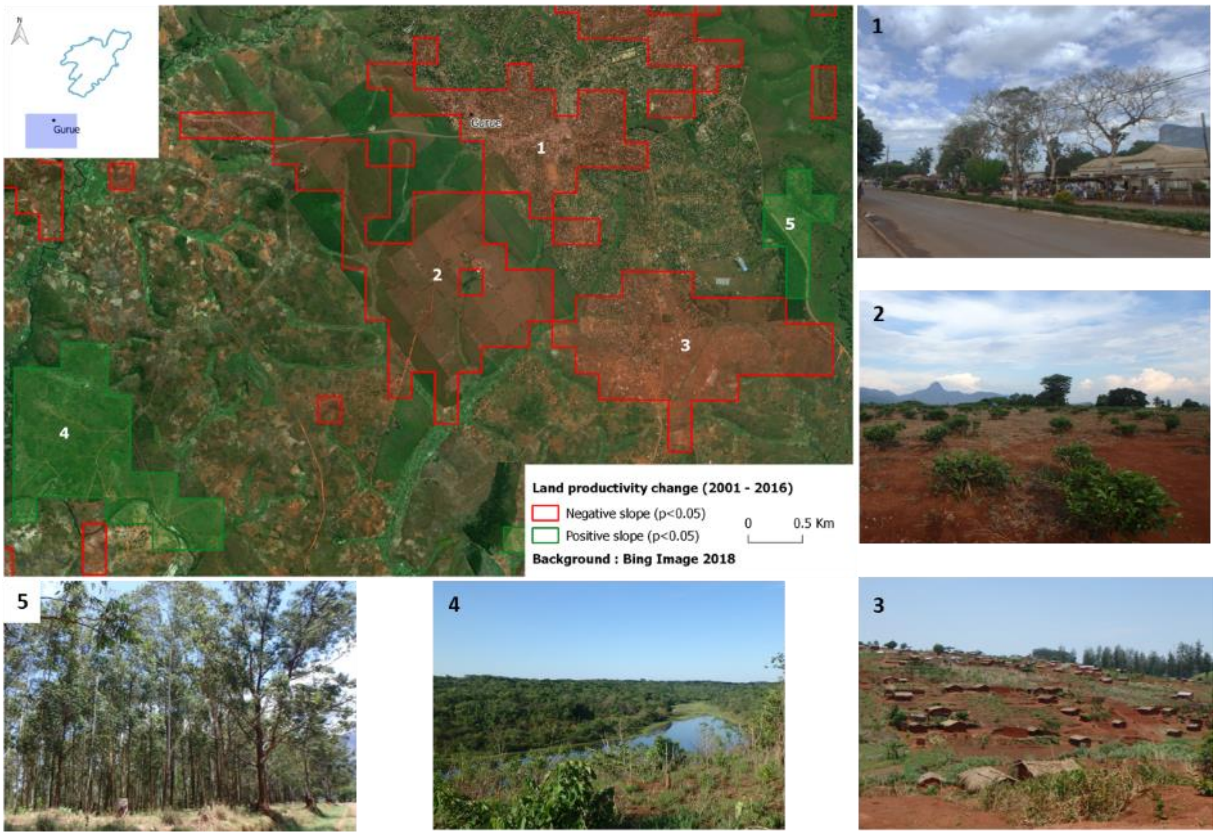

Figure 9 : Areas of significant land productivity change in Gurué. The red and green large pixels indicate areas of decreasing and increasing land productivity, respectively, as assessed using MODIS time series. The numbered ground photos illustrate the LULC of green and red areas samples: 1) Urban densification in Gurué city (red); 2) Old tea plantation still under exploitation, but degraded (red); 3) Settlement on an old tea plantation (red); 4): Post-agriculture forest regeneration (green); 5) Eucalyptus plantation (green)

4.2.3. Land productivity increase factors

The increase in land productivity is almost entirely driven by human factors (Figure 10, Table 4). This increase can be mainly explained by secondary vegetation regrowth (52.6% of the total increase trend) and agricultural productivity increase of fallow regrowth (23.3%).

Field observations showed that areas of increase of land productivity mainly correspond to cropland abandoned after cultivation, eucalyptus plantations or areas left fallow by tea companies to produce wood for fuel for factories (tea drying process) (Figure 6). To the west of the Namuli core area, areas of land productivity increase are past pastures used by the Portuguese and currently being abandoned. The increase could therefore be linked to the regeneration of woody species due to a grazing pressure decrease.

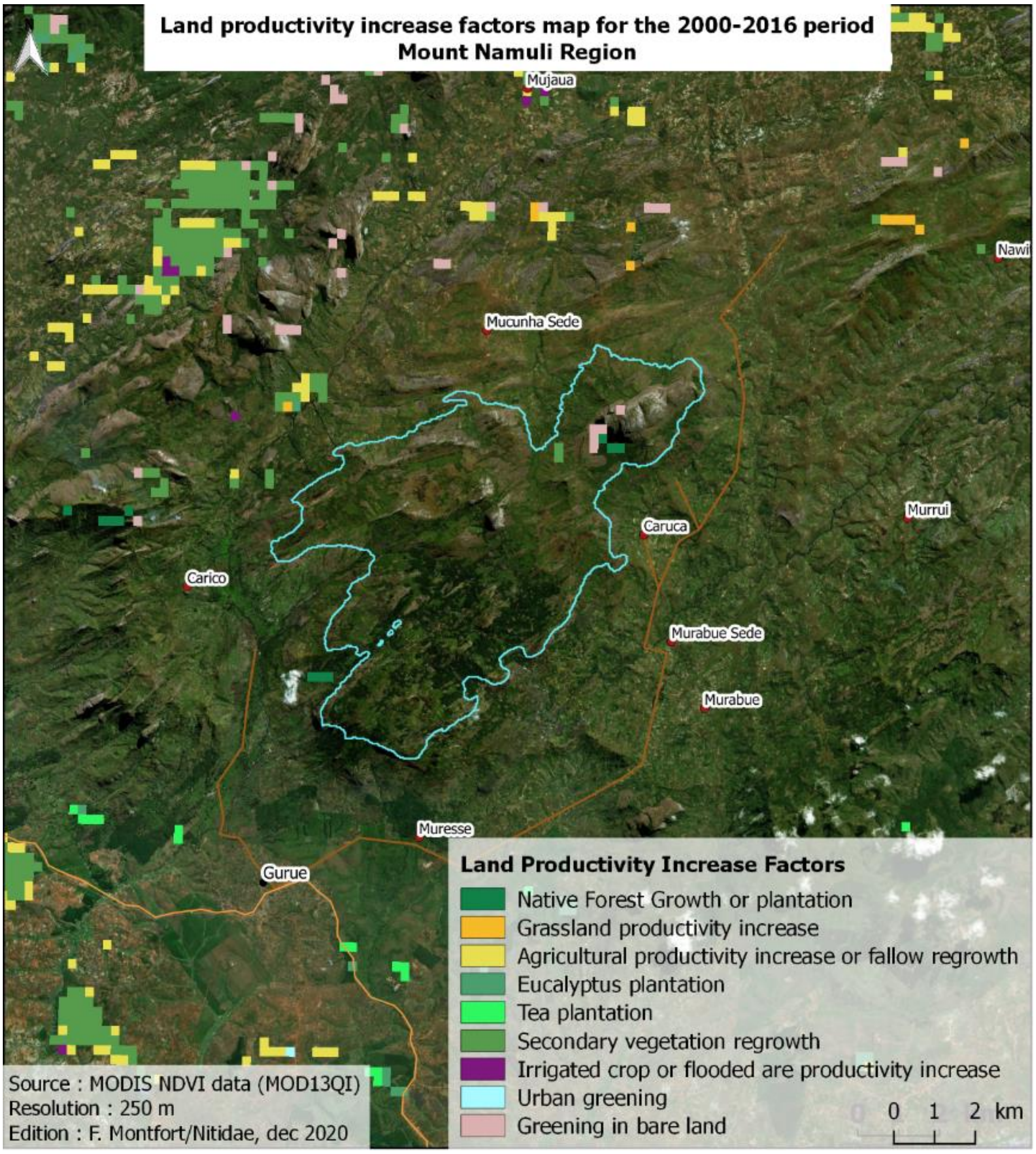

Figure 10 : Spatial distribution of the main drivers of land productivity increases.

Table 4: Distribution of main factors of land productivity increases

Land productivity factors	Hectares	% increase
Secondary vegetation regrowth	1 327	52,6
Agricultural productivity increase or fallow regrowth	589	23,3
Greening in bare land	246	9,7
Eucalyptus plantation	121	4,8
Tea plantation productivity increase	88	3,5
Grassland productivity increase	60	2,4
Native Forest Growth or plantation	51	2,0
Irrigated crop or flooded are productivity increase	37	1,5
Urban greening	5	0,2

5_Analysis of historical deforestation

Historical deforestation analysis helps to better understand past dynamics and therefore provide appropriate options to reduce deforestation. The objective of this section is to map moist evergreen forest extent and deforestation over a 20 years period from 2000 to 2020 in the Namuli core area. This section describes the various steps that have been implemented for the analysis of past deforestation, from the acquisition of satellites images to the final results.

5.1. Methodology :

The methodology used in this study is based on a classical approach of remote sensing: 1) satellite image collection, 2) data pre-processing, 3) delineation of training plots, 4) supervised classification of land use and land cover change using a statistical model and 5) post-processing. The methodology is summarized in the following figure:

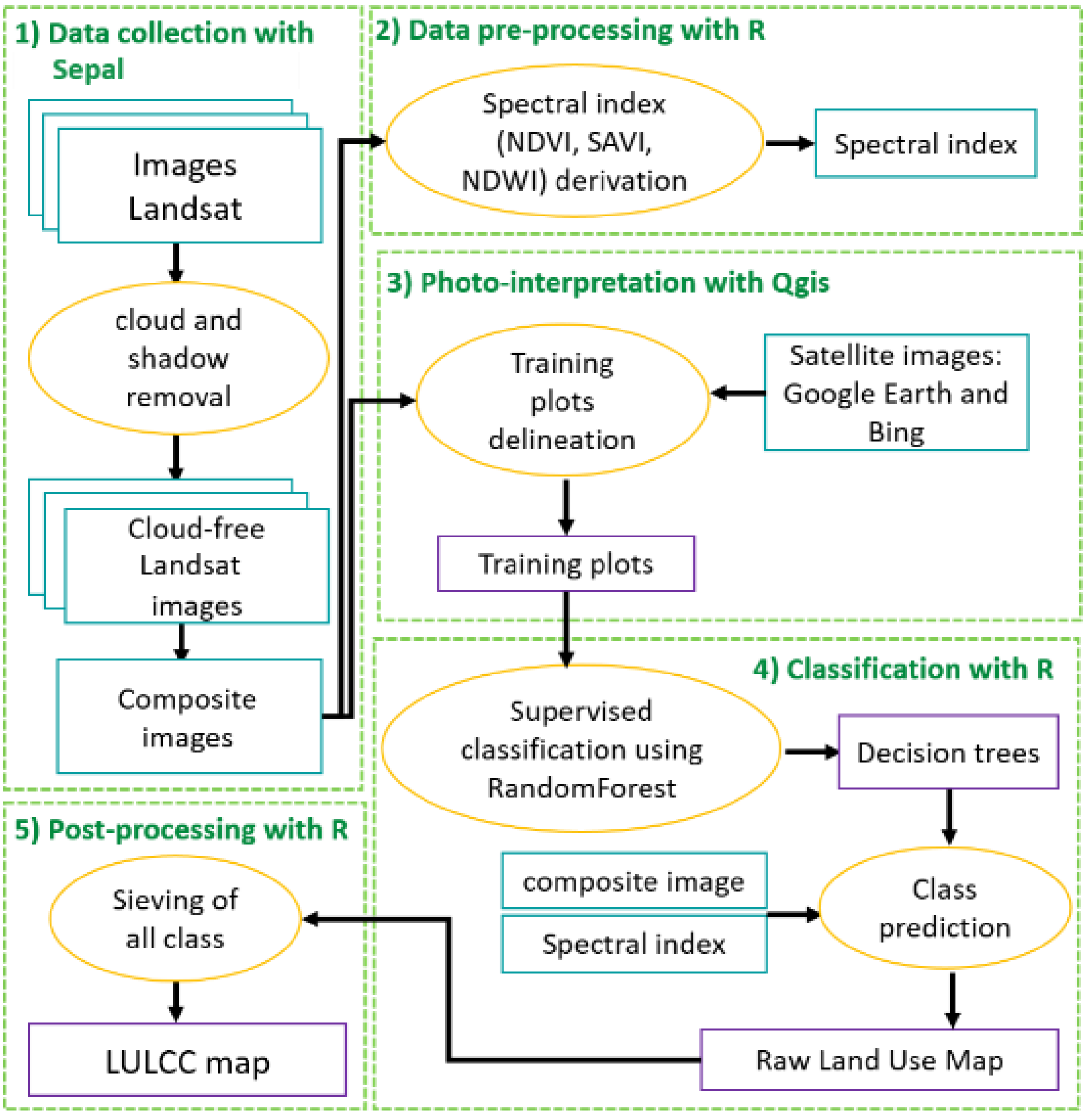

Figure 11 : Processing chain applied for the land use and land cover change mapping

5.1.1. Satellite image collection

The land use and land cover change analysis relies on Landsat imagery as it is the only consistent source of high resolution satellite data available for the period of interest. Landsat images from 2000 to 2020 were used with a spatial resolution of 30 m. Those images are available on the USGS data servers (Earth Explorer, www.earthexplorer.usgs.gov) for free. When there was no cloud-free image available we used the Sepal platform (https://sepal.io) to create a cloud-free Landsat composite. All images come from three different Landsat missions: 5, 7 and 8/OLI, which have slightly different sensors in terms of width and number of spectral bands. Images were uploaded by bands; therefore it was primarily necessary to combine these single bands into multispectral images (stacking) to be comparable from one date to another.

The study area is covered by one Landsat scene, presenting the following identifiers: 166/71 (path/row). The selected Landsat scenes are presented in the following tables.

Table 5 : Date of selected LANDSAT image

Year	Satellite	Sensor	Date of acquisition	Spatial resolution (m)	Scene cloud cover (%)
2000	Landsat 7	ETM+	27/04/2000	30	1
2005	Landsat 5	TM	22/07/2005	30	0
2009	Landsat 5	TM	30/05/2009	30	0
2013	Landsat 8	OLI/TIRS	10/06/2013	30	1
2015	Landsat 8	OLI/TIRS	16/06 & 18/07/2015	30	3 & 7
2018	Landsat 8	OLI/TIRS	08/06 & 26/07/2018	30	1
2020	Landsat 8	OLI/TIRS	13/06/2020	30	9

To ensure good geometrical quality images, Landsat Global Land Survey products (GLS) and Level-1T (L1T) were used. These data have sufficient radiometric and geometric qualities to perform land use change analysis. Additionally, we performed a visual inspection of each scene to check their geometric consistencies. No additional geo-rectification was performed.

5.1.2. Data pre-processing and variables

In order to improve the classification and increase the spectral differentiation between categories, several spectral indexes were derived from the primary bands of the satellite images, as presented in the following table.

Table 6 : Spectral indexes calculated

Index	Formula	References
NDVI (Normalized Difference Vegetation Index) – Vegetation spectral enhancement	NDVI=(NIR-R)/(NIR+R)	Rouse et al., 1974
SAVI (Soil Adjusted Vegetation Index) – Soil spectral enhancement	SAVI = (NIR - R) / (NIR + R + L) * (1.0 + L)	Huete, 1988
NDWI (Normalized Difference Water Index) – Water spectral enhancement	NDWI = (NIR - SWIR) / (NIR + SWIR)	Gao, 1996

5.1.3. Delineation of training plots

After data pre-processing, the method to establish a deforestation map follows three main steps:

- Definition of land use and land cover classes;

- Delimitation of training plots;
- Classification with a specific algorithm (Random Forest).

<u>Definition of land use and land cover changes classes</u>

Land use (LU) categories that exist in the areas and are detectable with Landsat imagery and land cover change categories (LCC – 6 period of deforestation) are presented in the following table:

Table 7 : Typology of land use and land cover categories for the study

<table>
<tr><th>Code</th><th colspan="2">Name</th><th>Description</th></tr>
<tr><td>1</td><td rowspan="9">Land Use and Land Cover 2020</td><td>Forest</td><td>Forest includes all land with dense mature woody vegetation (mainly moist evergreen forest) that have not been perturbed.</td></tr>
<tr><td>2</td><td>Grassland</td><td>Grassland is an area with herbaceous plant types, but without crop cultivation. Trees and shrubs can be present but cover is less than 10%.</td></tr>
<tr><td>3</td><td>Mosaic of culture and young fallow</td><td>This classe includes land covered with temporary crops followed by harvest and a period of bare soil or fallow.</td></tr>
<tr><td>4</td><td>Plantation</td><td>Plantation (Tea, Eucalyptus, Macadamia)</td></tr>
<tr><td>7</td><td>Secondary vegetation</td><td>Secondary vegetation is regenerated forest that has been disturbed by human activities.</td></tr>
<tr><td>8</td><td>Irrigated crop / Flooded area</td><td>Lowland irrigated crop or flooded area</td></tr>
<tr><td>9</td><td>Water</td><td>This class includes areas covered by water during all the year.</td></tr>
<tr><td>10</td><td>Urban area, Settlement</td><td>Urban area and settlement comprises all developed land, including areas of human habitation and transportation infrastructure.</td></tr>
<tr><td>11</td><td>Bare soil, rock, sands an others</td><td>This class includes bare soil, rock, and all unmanaged land areas that do not fall into any of the previous classes.</td></tr>
<tr><td>12</td><td rowspan="6">Land Cover Change 2000-2020</td><td>Deforestation between 2000-2005</td><td rowspan="6">Clearing of forest areas by cutting down the trees</td></tr>
<tr><td>13</td><td>Deforestation between 2005-2009</td></tr>
<tr><td>14</td><td>Deforestation between 2009-2013</td></tr>
<tr><td>15</td><td>Deforestation between 2013-2015</td></tr>
<tr><td>16</td><td>Deforestation between 2015-2018</td></tr>
<tr><td>17</td><td>Deforestation between 2018-2020</td></tr>
</table>

Delimitation of training plots

Delimitation of training plots is a necessary step to calibrate the classification algorithm when applying a supervised classification. **The accuracy of the classification mainly depends on the quality of the delimitation of these training plots.** Polygons that represent land uses (LU) in 2020, as well as land cover changes (LCC) between each period, were delineated. Therefore, a standardized and rigorous photo-interpretation work was conducted. Photo-interpretation was carried on the basis of field knowledge, Landsat image patterns and high-resolution images from *Google Earth*. **Finally, 665 plots were delineated (see table below).**

Table 8 : Number of polygons and associated delineated area used as training plots

LULC Class ID			Number of training polygons	Cumulated area (ha)	Average size (ha)
1	Land Use and Land Cover 2020	Forest	55	104	1.9
2		Grassland	29	53	1.8
3		Mosaic of culture and young fallow	68	546	8.0
4		Plantation	124	1019	8.2
7		Secondary vegetation	61	188	3.1
8		Irrigated crop / Flooded area	41	124	3.0
9		Water	31	10	0.3
10		Urban area, Settlement	35	231	6.6
11		Bare soil, rock, sands an others	51	234	4.6
12	Land Cover Change 2000-2020	Deforestation between 2000-2005	8	3	0.4
13		Deforestation between 2005-2009	14	6	0.4
14		Deforestation between 2009-2013	23	12	0.5
15		Deforestation between 2013-2015	34	15	0.4
16		Deforestation between 2015-2018	59	24	0.4
17		Deforestation between 2018-2020	32	11	0.4
All			665	2582	3.9

First, in order to improve the localization and determination of changes, those areas were highlighted by performing a multi-dates color composite. Then, training plots were located in clusters *i.e.* by grouping several plots of different categories on a same landscape unit or small area. In order to reduce noise in training data, plots contours were verified by superposition on very high-resolution images available on *Google Earth*.

5.1.4. Supervised classification

Afterward, the training plot spatial database was correlated with the multi-date stacked image database using a statistical algorithm. The RandomForest algorithm, developed by Breiman (2002) and available in R software was used. It is a data-mining algorithm that combines bugging techniques and decision trees. It was successfully applied in land cover change studies in humid forests of Madagascar (Grinand et al., 2013) and in the Miombo forest biome (Kamusoko et al., 2014). First, the RandomForest algorithm must be calibrated to predict the different land-use categories to be classified. The calibration of the model is done from the database regrouping the previously delimited training plots.

5.1.5. Post-classification treatments

After classification, some isolated pixels were found, giving a noisy appearance to the map. Those isolated pixels were removed with the GDAL sieve filter (pixel connections: 4) in Qgis and replaced with the classification of the majority class that surrounds it, during post-classification processing. Remove only isolated pixels makes it possible to keep information on deforestation over small areas that would be removed with a stronger filter. Furthermore data concerning rivers extracted from the MNT with the Grass *r.watershed* tool were added to the map.

5.1.6. Deforestation rate calculation

In a first approach, an annual deforestation rate is a ratio between the deforestation area over a period and the number of years between the two dates of the same period (Menon and Bawa 1997). However, several publications explained that this simple ratio could not be used as deforestation rate dynamics followed a compound interests rule because the ratio changed with forest area during the period of interest as deforestation continued (Puyravaud 2003). Hence, an adaptation of this law was done to calculate annual deforestation rate. The following standardized equation proposed by Puyravaud (2003) was used in the present study:

$$\theta = -\frac{1}{t2 - t1} \ln \frac{A2}{A1}$$

Where A_i is the forest area during the year t_i.

This calculation approach requires knowing exactly the interval between the two dates (t1 and t2) of the considered period. Therefore, a table summarizing the exact interval between images was established (Table 9).

Table 9 : Time interval between reference year

Period		Time interval (decimal year)	
		Day	Year
27/04/2000	22/07/2005	1912	5.24
22/07/2005	30/05/2009	1408	3.86
30/05/2009	10/06/2013	1472	4.03
10/06/2013	18/07/2015	768	2.10
18/07/2015	26/07/2018	1104	3.02
26/07/2018	13/06/2020	688	1.88

5.2. Results

5.2.1. Forest cover and historical deforestation maps

Deforestation map and forest cover maps for each date of analysis are presented in Figure 12, 13 and 14. Forest cover loss started mainly in the south of the Namuli core area during the 2009-2013 period and the forest cover was gradually fragmented (Figure 14). Forest loss patch size was small, often less than half a hectare. In 2020, forests on the Namuli massif are significantly fragmented.

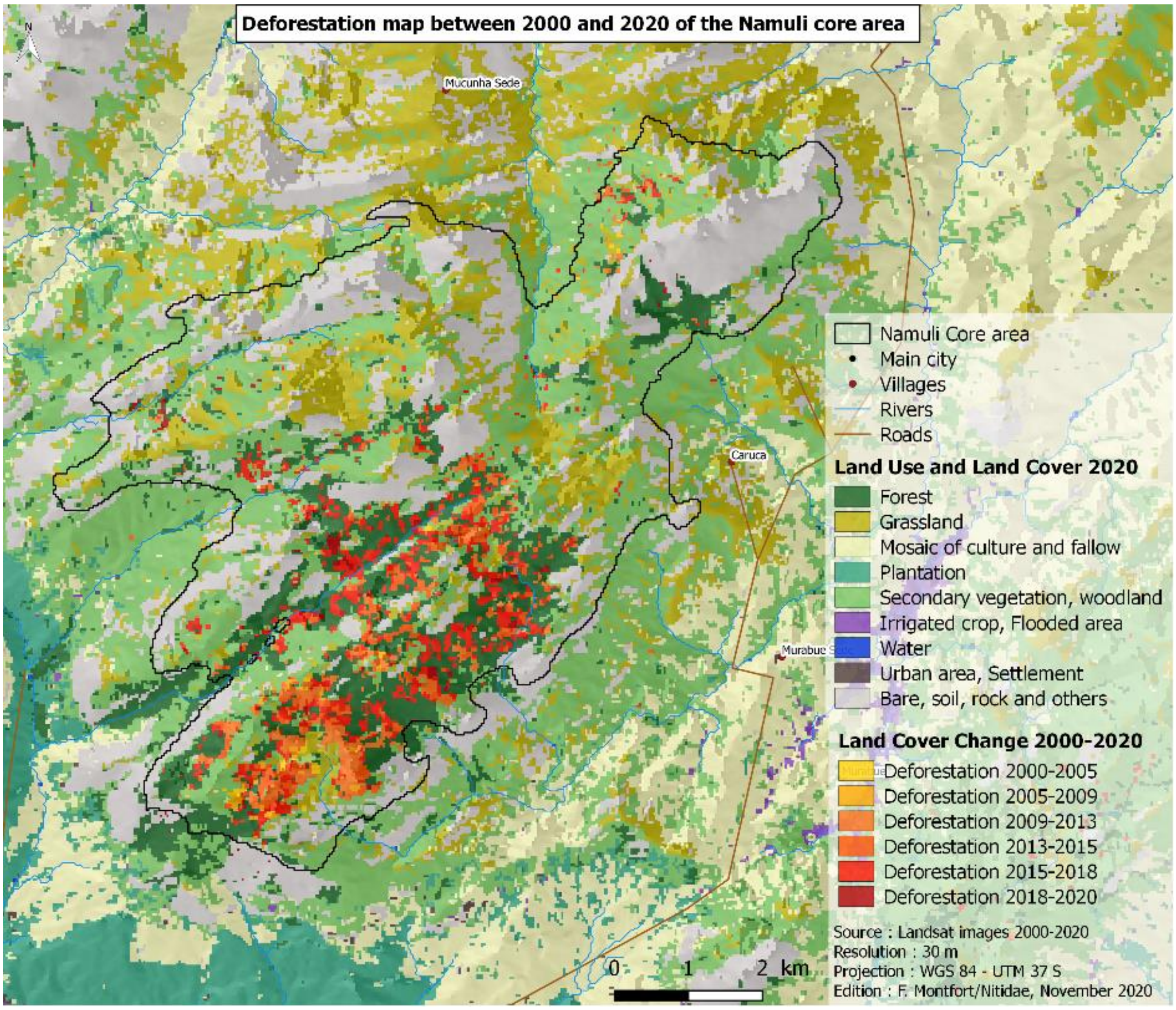

Figure 12 : Deforestation map between 2000 and 2020 of the Namuli core area

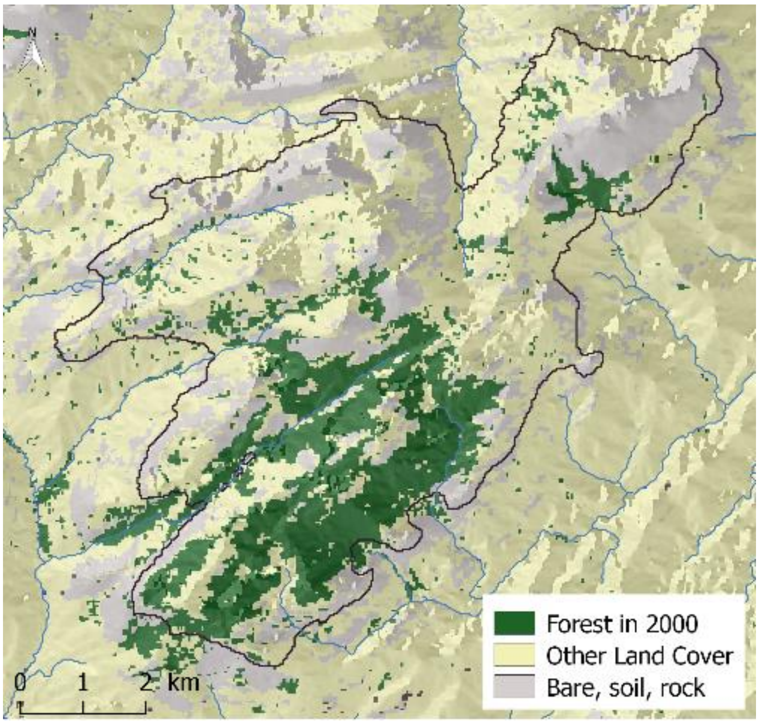

Figure 13: Forest cover in 2000 of the Namuli core area

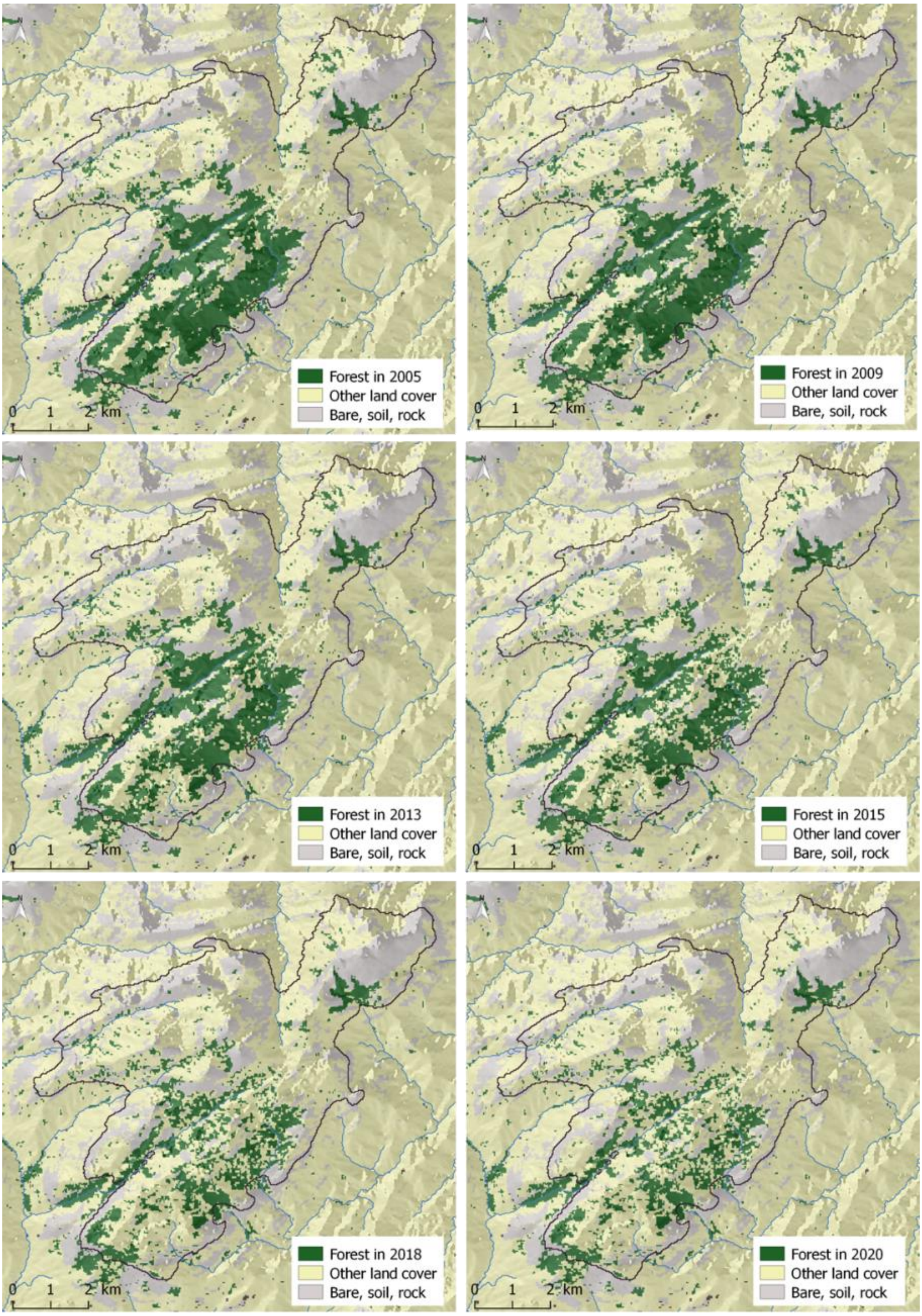

Figure 14 : Forest cover in 2005, 2009, 2013, 2015, 2018 and 2020 of the Namuli Core area

5.2.2. Forest and deforestation statistics

Forest and deforestation statistics extracted from the deforestation map are presented in the tables 10 and 11. **More than 40% (i.e. 568 ha) of the forested areas in the Namuli core area was lost between 2000 and 2020 (Figure 15)**. Indeed, forest cover in 2000 was estimated at 1351 ha (26.9 % of the total area) and, in 2020 remaining forest patches in the Namuli core area are estimated at 783 ha (15.6 % of the total area) (Table 10). **The Namuli core area had suffered important deforestation since mainly 2009, losing on average 48 ha per year, between 2009 and 2020 – this is an average annual deforestation rate of 4.7%** (Table 11). At the present rate of loss the remaining forest can be expected to be exhausted within 16 years. However, results show a decrease of deforestation rate (2.1 %) over the last analysis period 2018-2020 (Table 11 and Figure 16).

Table 10 : Forest statistics in the Namuli core area

Years	Forest area (ha)	% total area
2000	1351	26.9
2005	1339	26.7
2009	1323	23.3
2013	1187	23.7
2015	1053	21.1
2018	814	16.2
2020	783	15.6

Table 11 : Historical deforestation in the Namuli core area between 2000 and 2020

Period	Cumulative deforestation from 2000 (ha)	% forest lost compared to 2000	Annual forest loss (ha/an)	Annual deforestation rate (%)
2000 - 2005	12	0.9	2.3	0.2
2005 - 2009	28	2.1	4.2	0.3
2009 - 2013	164	12.1	33.6	2.7
2013 - 2015	298	22.1	64.1	5.7
2015 - 2018	537	39.7	78.8	8.5
2018 - 2020	568	42.1	16.8	2.1
2000 - 2020	**568**	**42.1**	**33.3**	**3.2**

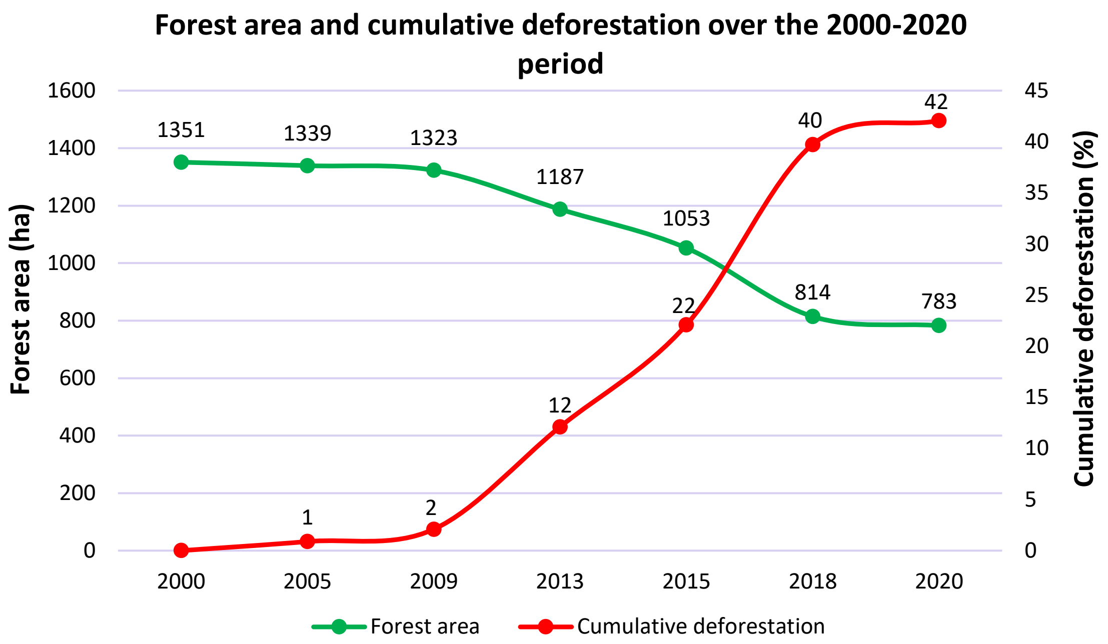

Figure 15 : Forest area and Cumulative deforestation over the 2000-2020 period in the Namuli core area

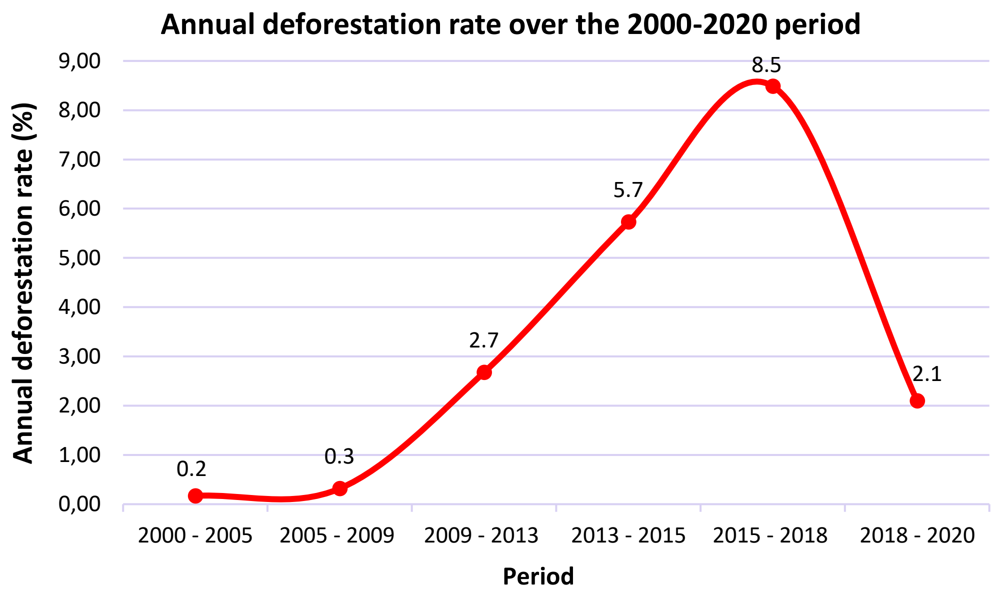

Figure 16 : Annual deforestation rate over the 2000 – 2020 period

6_Identification of most threatened forests

In this section, we address the question of the location of most threatened forests and therefore of the future deforestation, starting from the assumption that deforestation is not a random phenomenon but occurs in locations that combine advantageous bio-geophysical and socio-economic attributes for deforestation agents. For instance, soil fertility and distance from forested areas, transportations or markets are likely to influence the choice of human settlement and agricultural practices, putting natural forest location at various levels of risk.

6.1. Methodology

The methodology is based on Grinand et al. (2019) method. We use a machine learning algorithm (RandomForest) combined with datasets of potential spatial deforestation factors to provide a map of deforestation risk.

First, ten potential explanatory variables of deforestation were converted into spatially explicit layers and included in the analysis (Table 12). These variables are related to accessibility: distance to Gurue, villages and road, distance to forest edge; and natural constraints: slope, aspect, elevation, distance to river, soil moisture (estimated using the Topographic Wetness Index – TWI), and distance to rock (use as a proxy of soil depth). Then, an analysis of drivers of deforestation was conducted, using extractions of spatial predictor values. We analyze the relative importance of each variable by testing the correlation between (i) observed deforestation derived from the historical deforestation analysis (see Analysis of historical deforestation section) and (ii) datasets of geo-referenced deforestation factors. We used a stratified random sampling scheme by randomly sampling 1000 points in forest loss patches and 1000 points in forest. A datasets of 2000 observations were compiled. We also used a linear regression model to assess the importance of each variable. Finally, an ensemble model was calibrated using the datasets to predict and map deforestation risk (or probability of deforestation) based on the potential explanatory variables. The methodology is summarized in figure 17.

Figure 17: Processing chain applied for the deforestation risk mapping

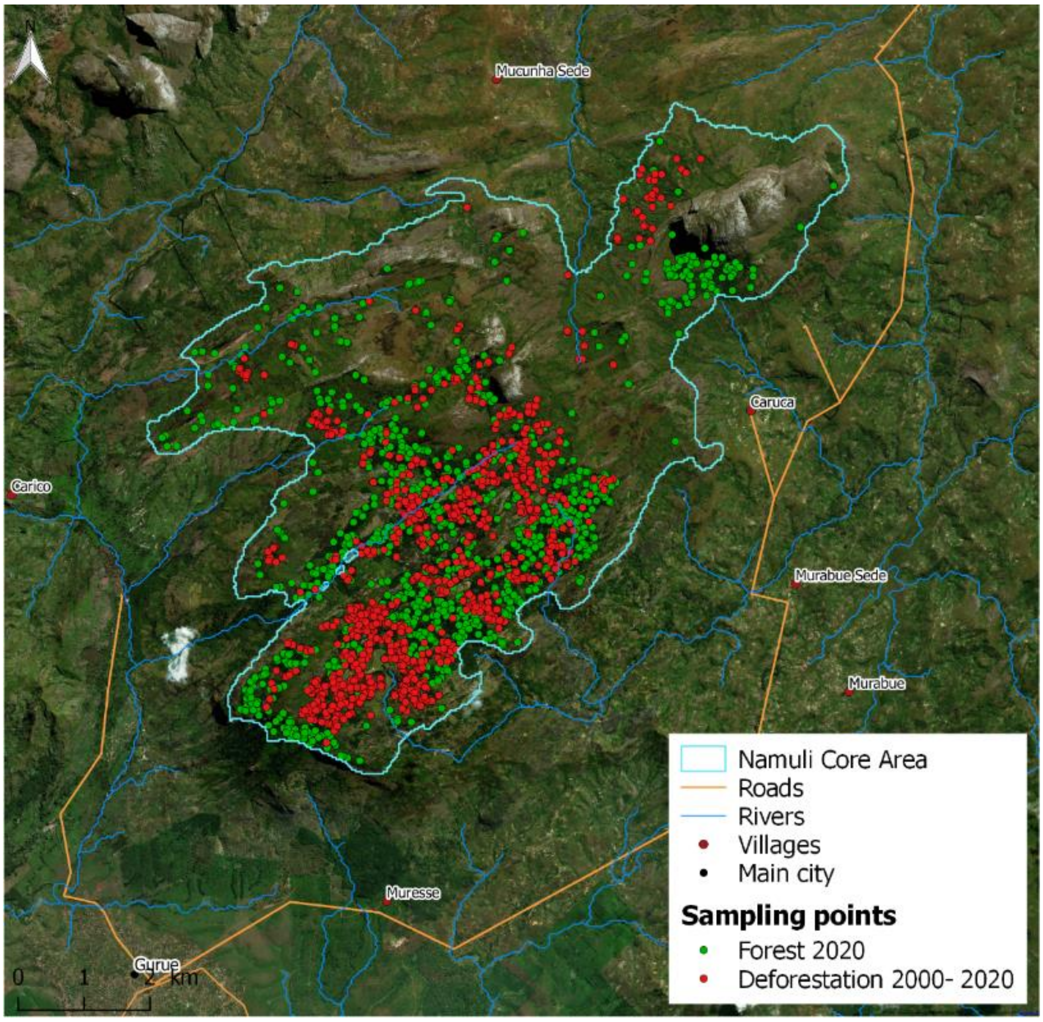

Figure 18: Sampling points in forest 2020 and deforestation between 2000 and 2020 and other potential explanatory variables

Table 12 : Potential drivers of deforestation used in the analysis

Name	Description	Source	Range	Unit
Slope	Slope	SRTM 30	0 - 79	%
Aspect	Exposition	SRTM 30	0 - 360	Degree
TWI	Topographic Wetness Index	SRTM 30	4 - 15	
Elevation	Elevation	SRTM 30	1538 - 2362	Metre
Dist city	Distance to Gurue	WB	3.2 – 15.6	Km
Dist_village	Distance to small villages	Nitidae	0.7 – 5.7	Km
Dist roads	Distance to road	Nitidae	0.6 – 6.3	Km
Dist rivers	Distance to rivers	SRTM 30	0 – 1.6	Km
Dist forest edge	Distance to forest edge	Nitidae	0 - 852	Metre
Dist rock	Distance to rock	Nitidae	0 – 410	Metre

6.2. Results

6.2.1. Drivers importance

The importance of factors was analyzed using a regression method to assess the relation between observed deforestation and the selected potential drivers (Table 13). Among the 10 potential drivers, slope, distance to road and village and soil moisture (TWI) were the most important.

Slope was the first driver explaining deforestation in this study. Deforestation is more likely to occur in low slope areas (<13 % - 7.4 °) (Figure 19). We observed that the forest patches closest to roads and villages are not the most deforested. However, in this analysis distances represent distances as the crow flies and do not take into account accessibility constraints to the highlands. Indeed, farmers will take the easiest paths to reach highlands and these paths do not always give access to the nearest forest patch. This can also be related to the selection of the most suitable areas for cultivation by farmers. Accessible but not deforested forests are probably those with shallow soils (shallow granitic bedrock) and little organic matter. We observed a slight increase of deforestation in areas with low soil moisture.

Deforestation occurs inside the forest patches between 100 and 250 m from the forest edge and not close to it, this leads to high forest fragmentation. This farmer's strategy is unusual because it is easier to clear-cut the forest at the edge than inside the forest. Deforestation is more likely to occur more than 60 m from the rocks where soils are deeper.

Table 13 : Results of linear logistic regression

	Estimate	Std. Error	z value	Pr(>|z|)	
(Intercept)	4.324e+00	1.787e+00	2.420	0.0155	*
Slope	-7.657e-02	8.624e-03	-8.878	< 2e-16	***
Aspect	-2.021e-04	6.076e-04	-0.333	0.7395	
Twi	-2.753e-01	4.979e-02	-5.528	3.24e-08	***
Elevation	-4.478e-04	8.793e-04	-0.509	0.6106	
Dist city	-1.223e-04	2.632e-05	-4.648	3.36e-06	***
Dist village	-6.403e-04	1.033e-04	-6.199	5.68e-10	***
Dist road	8.984e-04	1.117e-04	8.040	8.96e-16	***
Dist rivers	-4.003e-04	3.270e-04	-1.224	0.2209	
Dist forest edge	-3.998e-03	9.165e-04	-4.363	1.28e-05	***
Dist rock	3.302e-03	7.865e-04	4.199	2.68e-05	***

Linear influence

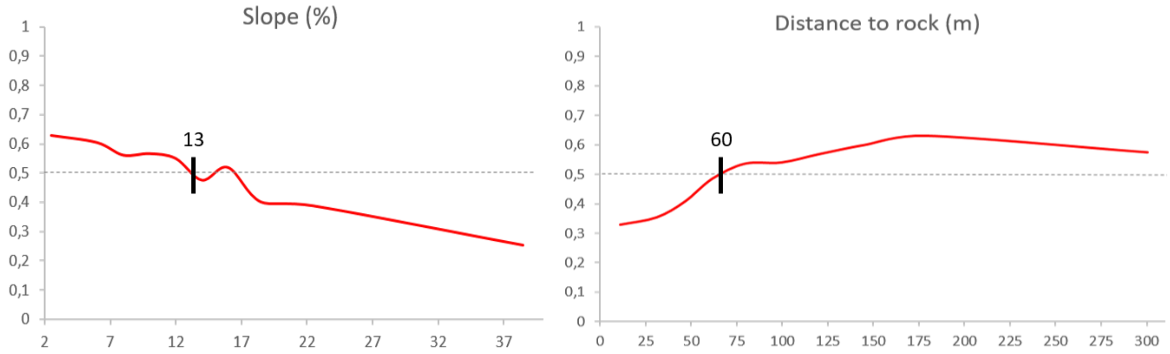

Influence zonal

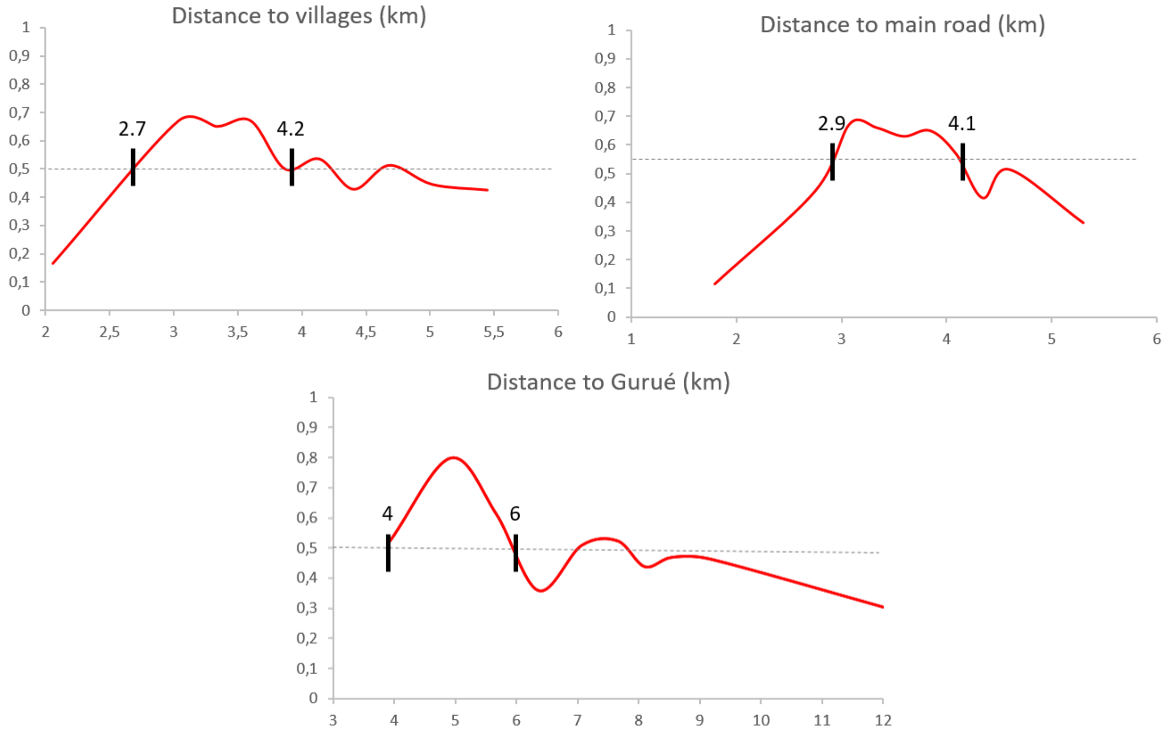

Low influence

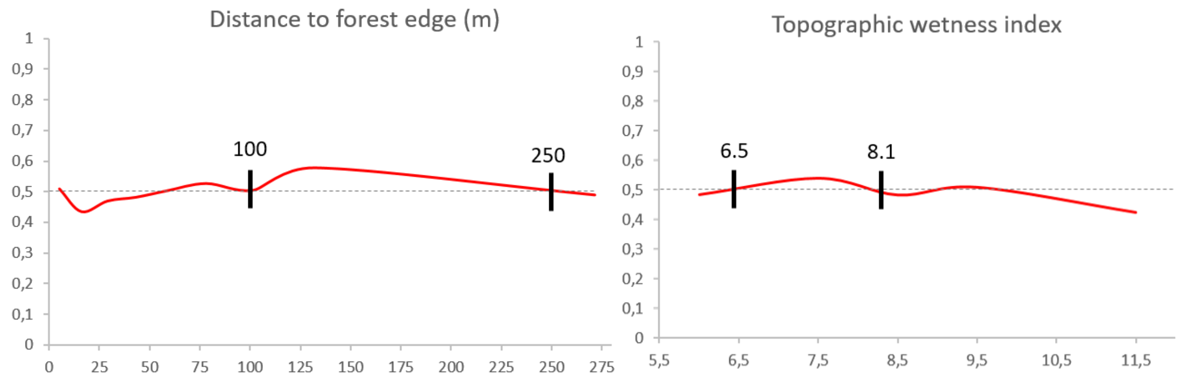

Figure 19 : Probability distribution of deforestation observation. The dashed line represents the 50% probability (value above indicates high probability of deforestation).

6.2.2. Deforestation risk map

Deforestation risk map is presented in Figure 20. **A large part of the remaining moist evergreen forest patches present a high risk of deforestation (17% of the remaining forest patches present a deforestation probability greater than 50%).** Forest patches with low deforestation probability are mainly those located in steep areas (> 13%), as forest patches located near Mount Namuli. The most important one being the Khali forest, protected by local community decision.

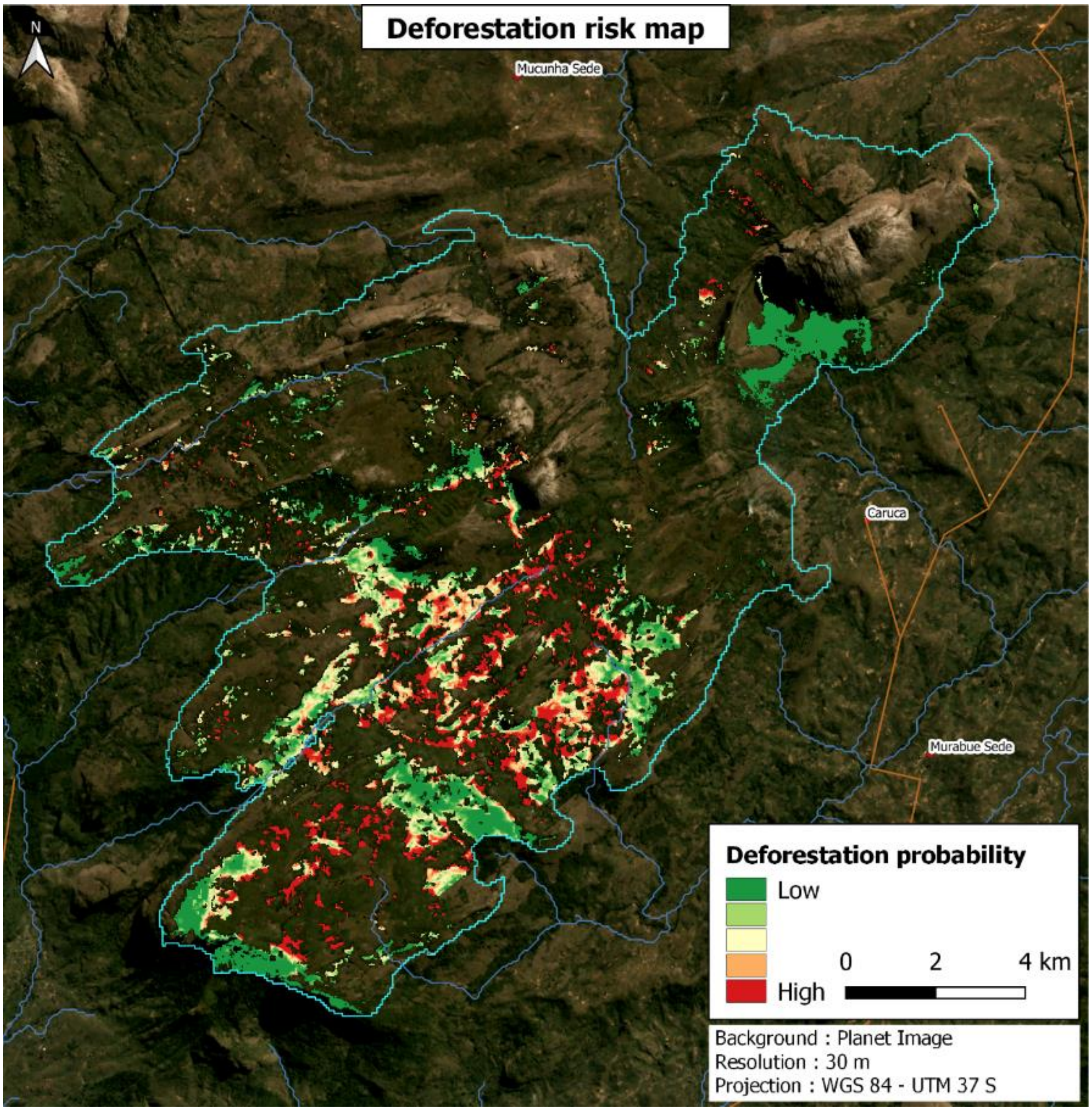

Figure 20: Deforestation risk map

7_ References

Breiman, L., 2001. Random Forest, Machine Learning, 45(1): pp 5-32.

Governo de Moçambique. 2016. Estratégia Nacional para a Redução de Emissões de Desmatamento e Degradação Florestal, Conservação de Florestas e Aumento de Reservas de Carbono Através de Florestas (REDD+) 2016-2030. Maputo: Ministério da Terra, Ambiente e Desenvolvimento Rural, 02 de Novembro de 2016

Grinand, C., Rakotomalata, F., Gond, V., Vaudry, R., Bernoux, M., and Vieilledent, G., 2013. Estimating deforestation in tropical humid and dry forests in Madagascar from 2000 to 2010 using multi-date Landsat satellite images and the random forest classifier. Remote sensing of Environment, 139: 68-80.

Grinand, C., Vieilledent, G., Razafimbelo, T., Rakotoarijaona, J.R., Nourtier, M., Bernoux, M., 2019. Landscape-scale spatial modelling of deforestation, land degradation and regeneration using machine learning tools. Land Degradation & Development. doi:10.1002/ldr.3526

Kamusoko, C., Gamba, J., and Murakami, H., 2014. Mapping Woodland Cover in the Miombo Ecosystem: A Comparison of Machine Learning Classifiers. Land 3 (2): 524–40.

Montfort, F, Bégué, A, Leroux, L, Blanc, L., Gond, V., Cambule, A.H., Remane, I.A.D, Grinand, C.. From land productivity trends to land degradation assessment in Mozambique: Effects of climate, human activities and stakeholder definitions. Land Degrad Dev. 2020; 1– 17. https://doi.org/10.1002/ldr.3704

Montfort, F., & Grinand, C., 2020. Land Use and Land Cover Map of Mount Namuli and surroundings in Mozambique [Data set]. Zenodo. http://doi.org/10.5281/zenodo.4121958

Puyravaud, J.P., 2003. Standardizing the Calculation of the Annual Rate of Deforestation. Forest Ecology and Management 177 (1): 593–96.

Timberlake, J.R., Dowsett-Lemaire, F., Bayliss, J., Alves T., Baena, S., Bento, C., Cook, K., Francisco, J., Harris, T., Smith, P. & de Sousa, C. (2009). Mt Namuli, Mozambique: Biodiversity and Conservation. Report produced under the Darwin Initiative Award 15/036. Royal Botanic Gardens, Kew, London. 114 p

List of figures

List of tables